Chiral *d*-wave superconductivity in a triangular surface lattice mediated by long-range interaction

Xiaodong Cao,[1] Thomas Ayral,[2,3] Zhicheng Zhong,[1,4] Olivier Parcollet,[3] Dirk Manske,[1] and Philipp Hansmann[1,5]

[1]*Max-Planck-Institut für Festkörperforschung, Heisenbergstrasse 1, 70569 Stuttgart, Germany*
[2]*Physics and Astronomy Department, Rutgers University, Piscataway, New Jersey 08854, USA*
[3]*Institut de Physique Théorique (IPhT), CEA, CNRS, UMR 3681, 91191 Gif-sur-Yvette, France*
[4]*Ningbo Institute of Materials Technology and Engineering, Chinese Academy of Sciences, 315201 Ningbo, China*
[5]*Institut für Theoretische Physik, Eberhard Karls Universität Tübingen, Auf der Morgenstelle 14, 72076 Tübingen*

(Received 9 October 2017; revised manuscript received 18 December 2017; published 20 April 2018)

Adatom systems on the Si(111) surface have recently attracted an increasing attention as strongly correlated systems with a rich phase diagram. We study these materials by a single band model on the triangular lattice, including $1/r$ long-range interaction. Employing the recently proposed TRILEX method, we find an unconventional superconducting phase of chiral d-wave symmetry in hole-doped systems. Contrary to usual scenarios where charge and spin fluctuations are seen to compete, here the superconductivity is driven simultaneously by both charge *and* spin fluctuations and crucially relies on the presence of the long-range tail of the interaction. We provide an analysis of the relevant collective bosonic modes and predict how a *cumulative* charge and spin paring mechanism leads to superconductivity in doped silicon adatom materials.

DOI: 10.1103/PhysRevB.97.155145

I. INTRODUCTION

The search for materials with unconventional high temperature superconductivity (SC) has been one of the most active fields in correlated solid state physics since the discovery of the cuprate high T_c compounds. Sophisticated synthesis technology nowadays allows for the construction of new materials like heterostructures or surface systems on an atomic length scale. Recently, many-body studies on experimentally well-controlled correlated adatom lattices X:Si(111) and X:Ge(111) with (X = Pb,Sn,C) led to interesting results [1–5] and allowed for the unification of the materials in a single phase diagram [3]. A first-principles derivation of the low-energy Hamiltonian of these systems [2,3] revealed sizable long-range interactions, explaining why the standard Hubbard model fails to capture the materials' ground states or low-energy spin and charge fluctuations. Depending on the species of the adatom, some of the materials were shown to be in close vicinity to a triple point between a Fermi liquid, a Mott insulator, and a charge-ordered insulator. Sn:Si(111) and Pb:Si(111) in particular turned out to be close to a charge-order Mott insulator phase transition with sizable charge fluctuations which, in the case of Sn:Si(111) were visible in core-level spectroscopy [5]. In complementary studies [4], the importance of spin fluctuations for Sn:Si(111) was emphasized. Silicon adatom systems with intrinsic long-range interactions are, hence, promising candidates to search for new physics like unconventional SC.

For such systems, theoretical methods are needed which are capable to capture both local and non-local electronic correlations. Dynamical mean-field theory (DMFT) [6,7] has been proven to be a powerful approach to treat local correlations and Mott physics. If nonlocal interactions have to be treated, extended DMFT (EDMFT) [8] captures their effects on the local self energy and charge polarization by a retarded onsite interaction. Local approximations like DMFT and EDMFT are, however, not sufficient when nonlocal fluctuations start to play an important role. To overcome these shortcomings of DMFT, several extensions have been proposed [9,10]. Cluster extensions of DMFT in real and reciprocal space [10–13], e.g., are capable to treat nonlocal short-range fluctuations. Long-range fluctuations, on the other hand, can be taken into account by DMFT+GW [14–16] or dual boson methods [17–20]. For our paper, we employ the recently developed TRILEX approximation [21–24], which combines a balanced treatment of long-range spin and charge fluctuations with comparatively little computational effort.

In this paper, we show that the triangular lattice model for the adatom materials has a dome-shaped superconducting phase of chiral d-wave symmetry as a function of hole doping in realistic parameter regimes. The long-range interaction is key for enhanced critical temperatures and distinguishes the adatom Hamiltonian from triangular Hubbard models [25–32]. By analyzing spin- and charge-response functions (and their dependence on the materials' long-range interaction), we further show that the pairing mechanism crosses over from a cumulative spin/charge fluctuation character at small dopings to a charge-dominated one at large doping.

II. MODEL AND METHOD

We make use of the extended Hubbard model on the triangular lattice with $1/r$ interactions,

$$H = \sum_{i,j,\sigma} t_{ij}\hat{c}^{\dagger}_{i\sigma}\hat{c}_{j\sigma} + \frac{1}{2}\sum_{i,j} U_{ij}\hat{n}_i\hat{n}_j - \mu\sum_i \hat{n}_i, \qquad (1)$$

to study the low-energy physics of adatom systems, following a first principles constrained random-phase approximation (cRPA) derivation [2] where $\hat{c}^{\dagger}_{i\sigma}$ ($\hat{c}_{i\sigma}$) are electron creation (annihilation) operators on site i with spin $\sigma = \uparrow,\downarrow$. $\hat{n}_i = \hat{n}_{i\uparrow} + \hat{n}_{i\downarrow}$ is the density operator on site i, and μ is the chemical potential. t_{ij} and U_{ij} are the hopping integrals and long-range Coulomb interaction strength between sites i and j.

For translational invariant two-dimensional systems, the long-range Coulomb interaction, in momentum space, reads $U_{\mathbf{q}} = U_0 + V\sum_{i\neq 0} e^{i\mathbf{q}\cdot\mathbf{R}_i}/|\mathbf{R}_i|$, where $\mathbf{R}_i$ are real space coordinates, U_0 is the on-site interaction, and V is the strength of the long-range interaction, respectively (Supplemental Material A in Ref. [33] and Ref. [34]). More specifically, we adopt hopping parameters up to next-nearest-neighbors ($t = 0.042$ eV and $t' = -0.02$ eV) from Refs. [2,3] derived from density-functional theory (DFT) for the Pb:Si(111) adatom system (closest to the triple point) and vary the interaction parameters in realistic regimes for the adatom materials found by cRPA [3].

TRILEX approximates the three-legged fermion-boson interaction vertex using a local self-consistent quantum impurity model. For systems retaining SU(2) symmetry, the self-consistent TRILEX equations [21–24] for the fermionic single particle self-energy $\Sigma(\mathbf{k}, i\omega_n)$ and bosonic polarization in charge and spin channel $P^{\mathrm{c,s}}(\mathbf{q}, i\nu_n)$ can be rewritten as

$$\Sigma_{\mathbf{k},i\omega_n} = \Sigma^{\mathrm{imp}}_{i\omega_n} - \sum_{\eta,\mathbf{q},i\nu_n} m^{\eta}\widetilde{G}_{\mathbf{k}+\mathbf{q},i\omega_n+i\nu_n}\widetilde{W}^{\eta}_{\mathbf{q},i\nu_n}\Lambda^{\mathrm{imp},\eta}_{i\omega_n,i\nu_n},$$

$$P^{\eta}_{\mathbf{q},i\nu_n} = P^{\mathrm{imp},\eta}_{i\nu_n} + 2\sum_{\mathbf{k},i\omega_n}\widetilde{G}_{\mathbf{k}+\mathbf{q},i\omega_n+i\nu_n}\widetilde{G}_{\mathbf{k},i\omega_n}\Lambda^{\mathrm{imp},\eta}_{i\omega_n,i\nu_n}, \quad (2)$$

where the index $\eta = \{\mathrm{c,s}\}$ corresponds to charge and spin channel, respectively, and ω_n and ν_n are fermionic and bosonic Matsubara frequencies. $G_{\mathbf{k},i\omega_n}$ is the dressed Green's function, and $W^{\mathrm{c,s}}_{\mathbf{q},i\nu_n}$ are the fully screened interactions in the charge and spin channels, respectively. The local part of self-energy and polarization are replaced by their impurity counterparts $\Sigma^{\mathrm{imp}}_{i\omega_n}$ and $P^{\mathrm{imp},\eta}_{i\nu_n}$, respectively, and for any quantity X, $\widetilde{X}_{\mathbf{k},i\omega_n} = X_{\mathbf{k},i\omega_n} - X^{\mathrm{loc}}_{i\omega_n}$ with $X^{\mathrm{loc}}_{i\omega_n} = \frac{1}{N_k}\sum_{\mathbf{k}\in\mathbf{B.Z.}} X_{\mathbf{k},i\omega_n}$. We employ the Heisenberg decomposition of the interaction [22], for which we have $m_{\mathrm{c}} = 1$, $m_{\mathrm{s}} = 3$, and $W^{\eta}_{\mathbf{q},i\nu_n} = U^{\eta}_{\mathbf{q}}[1 - U^{\eta}_{\mathbf{q}}P^{\eta}_{\mathbf{q},i\nu_n}]^{-1}$. Bare interactions in charge and spin channel are, hence, given by $U^{\mathrm{c}}_{\mathbf{q}} = \frac{U_0}{2} + v_{\mathbf{q}}$ and $U^{\mathrm{s}} = -\frac{U_0}{6}$ (for details see Supplemental Material A in Ref. [33]). This spin/charge ratio is a choice (dubbed "Fierz ambiguity" [22,24]). Moreover, in the parameter range explored in this paper, we have observed (Fig. 2 and Supplemental Material B in Ref. [33] and Ref. [35]) that using $\Lambda^{\mathrm{imp},\eta}_{i\omega_n,i\nu_n} \approx 1$ in Eq. (2) does not change our results qualitatively as it was also found in Ref. [23]. This simplified TRILEX version can be seen as a GW+EDMFT-like scheme which, however, can treat simultaneously both charge and spin fluctuations. The impurity problem was solved using the segment picture in the hybridization-expansion continuous time quantum Monte-Carlo algorithm [36–40] implemented with the TRIQS library [41].

To probe SC instabilities, we solve the linearized gap equation with converged simplified TRILEX results as an input [23]. For singlet d-wave pairing, the corresponding eigenvalue equation for the gap reads

$$\lambda\Delta_{\mathbf{k},i\omega_n} = -\sum_{\mathbf{k}',i\omega'_n}\left|G_{\mathbf{k}',i\omega'_n}\right|^2\Delta_{\mathbf{k}',i\omega'_n}V^{\mathrm{eff}}_{\mathbf{k}-\mathbf{k}',i\omega_n-i\omega'_n}, \quad (3)$$

where the singlet pairing interaction is given by

$$V^{\mathrm{eff}}_{\mathbf{q},i\nu_n} = m^{\mathrm{c}}W^{\mathrm{c}}_{\mathbf{q},i\nu_n} - m^{\mathrm{s}}W^{\mathrm{s}}_{\mathbf{q},i\nu_n}, \quad (4)$$

and is therefore a combination of effective interaction in *charge and spin* channel. The SC instability occurs when the largest eigenvalue $\lambda = 1$. The pairing symmetry is monitored by the $\mathbf{k}$ dependence of the gap function $\Delta_{\mathbf{k},i\omega_n}$.

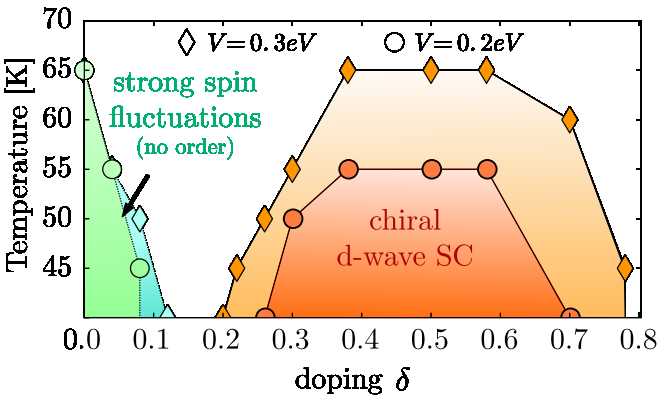

FIG. 1. Phase diagram of the Hamiltonian Eq. (1) as function of temperature (for $T > 40$ K) and doping for $U_0 = 0.7$ eV, $V = 0.2$ eV (circles) and $V = 0.3$ eV (diamonds). Green/blue regions correspond to $1 \geqslant \mathrm{Max}[-\mathrm{P^s}(\mathbf{q}, \mathrm{i}\nu_{\mathrm{n}} = 0)\mathrm{U^s}] \geqslant 0.95$ for $\mathbf{q} \in \mathbf{B.Z.}$ Orange/red regions indicate chiral d-wave superconductivity.

III. RESULTS

Emergence of d-wave SC. In Fig. 1, we plot the temperature–doping (T–δ) phase diagram for $V = 0.2$ eV and $V = 0.3$ eV for a fixed value of $U_0 = 0.7$ eV in the simplified TRILEX approximation. At half-filling ($\delta = 0$) we obtain a correlated Fermi liquid (Supplemental Material C in Ref. [33]) with strong magnetic fluctuations. The static spin-spin correlation function $\chi^{\mathrm{s}}(\mathbf{q}, i\nu_n = 0)$ is very large at some $\mathbf{q}$ but has not diverged yet, i.e., no phase transition has occurred. More precisely, we use $\mathrm{Max}[-\mathrm{P^s}(\mathbf{q}, \mathrm{i}\nu_{\mathrm{n}} = 0)\mathrm{U^s}]$ with $\mathbf{q} \in$ B.Z., which reaches 1 at a second-order spin-ordering phase transition to quantify the strength of the spin fluctuations and color code regions in the phase diagram for which $1 > \mathrm{Max}[-\mathrm{P^s}(\mathbf{q}, \mathrm{i}\nu_{\mathrm{n}} = 0)\mathrm{U^s}] \geqslant 0.95$ in green ($V = 0.2$ eV) and blue ($V = 0.3$ eV). From this plot, we see that spin fluctuations are slightly enhanced by increasing V. For $\delta > 0.2$ we observe the emergence of a dome-shaped superconducting phase (a plot of λ in Eq. (3) as a function of temperature is shown in the Supplemental Material D in Ref. [33]). The pairing symmetry of the SC phase is of d-wave character and includes doubly degenerate $d_{x^2-y^2}$- and d_{xy}-wave pairing channels (see Supplemental Material E in Ref. [33] and Ref. [42] for a plot of the gap function). The degeneracy of these two pairing symmetries is protected by the $\mathrm{C_{6v}}$ point group of the triangular lattice, which then yields chiral d-wave symmetry below $\mathrm{T_c}$ to maximize condensation energy. The predicted chiral SC phase depends crucially on V: $\mathrm{T_c}$ increases from $V = 0.2$ eV (red circles) to $V = 0.3$ eV (orange diamonds) as shown in Fig. 1. Moreover, for $V = 0.0$ eV and $V = 0.1$ eV (not shown here), we do not find a SC phase for $T > 40$ K.

Impact of long-range interaction on susceptibilities and single particle spectra. The crucial impact of V on the SC instability is reflected in the effective singlet-pairing interaction $V^{\mathrm{eff}}_{\mathbf{q},i\nu_n}$, which depends on fluctuations in *both* charge and spin channels. We analyze the respective susceptibilities $\chi^{\mathrm{c/s}}(\mathbf{q}, i\nu_n)$ with the data shown in Fig. 2: In the upper panels

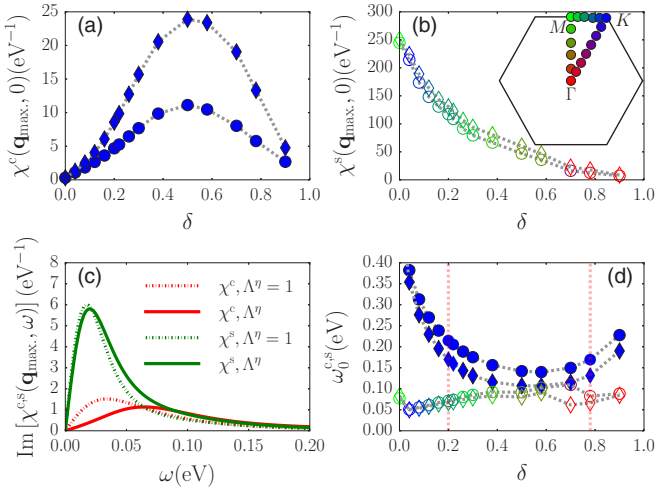

FIG. 2. Maximum values of the static charge (a) and spin (b) response functions versus hole doping. Color coding indicates the position of the maximum in the first Brillouin zone as defined in the inset. Data is shown for fixed $U_0 = 0.7$ eV and $T = 40$ K and nonlocal interaction strength $V = 0.3$ eV (diamonds) and $V = 0.2$ eV (circles). (c) Charge- and spin-response functions on the real frequency axis (obtained by analytical continuation with the maximum entropy method [43]) at their maximum in momentum space ($\mathbf{q}_{\max.}$) with (dashed) and without (solid) vertex corrections for $T = 116$ K and $\delta = 0.2$. (d) Characteristic frequency of charge (filled symbols) and spin (open symbols) fluctuations with the same convention and parameters as (a) and (b).

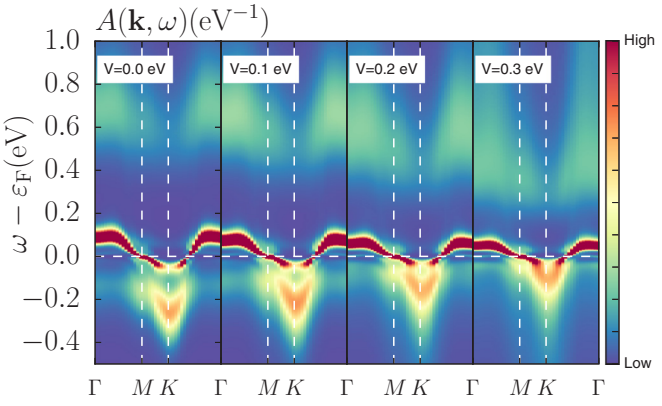

FIG. 3. Single particle spectral function $A(\mathbf{k},\omega)$ along the path Γ-M-K-Γ (see inset of Fig. 2) for fixed doping $\delta = 0.2$, $T = 40$ K, $U_0 = 0.7$ eV and four values of V.

we show the maximum values of the static ($i\nu_n = 0$) charge (left hand side) and spin (right hand side) susceptibilities as a function of hole doping. The corresponding position of the maximum in the first Brillouin zone is color coded (see inset).

The charge fluctuations increase with hole doping to a maximum value around $\delta = 0.5$ and, thereafter, decrease approaching the "empty" limit at $\delta = 1$. The spin fluctuations, instead, decrease monotonically as a function of δ. While $\chi^c(\mathbf{q}, i\nu_n = 0)$ always peaks at K, the maximum of $\chi^s(\mathbf{q}, i\nu_n = 0)$ moves from M to K when the system is slightly doped, and then follows $K \to M \to \Gamma$ when the system is further hole doped. The peak position of the charge response function as a function of doping remains at the K point since its momentum dependence is mainly determined by the doping-independent $v(\mathbf{q})$, which energetically favors a 3×3 charge configuration in real space [3]. The momentum dependence of the spin response function, however, is mostly determined by the topology of the Fermi surface. Indeed, the V dependence is much stronger for the charge response [compare diamond ($V = 0.3$ eV) and circle ($V = 0.2$ eV) symbols in Fig. 2]. There are, however, small effects of V to the spin-response function, which can be understood by the V-dependent renormalization of the one-particle spectra as show in Fig. 3 [44]. At fixed $T = 40$ K and $\delta = 0.2$, V is increased from 0.0 eV to 0.3 eV (subplots from left to right hand side). Upon increasing V, the bandwidth is effectively reduced and the spectral weight near to the Fermi energy is increased. Consequently, particle-hole excitations that contribute to the spin polarization $P^s(\mathbf{q}, i\nu_n)$ and the spin susceptibility are enhanced.

We now extend these considerations to the frequency dependence of the bosonic fluctuations. In Fig. 2(c), we plot the dynamic response functions at the $\mathbf{q}$-points where they are maximal ($\mathbf{q}_{\max.}$) for doping $\delta = 0.2$. The data clearly shows a peaked structure of the dynamic response functions. Moreover, we show in this plot the impact of the vertex corrections (compare solid and dashed lines). which are only quantitative in the considered case as claimed in the introduction. Figure 2(d) shows the doping dependence of the characteristic frequency $\omega_0^{c,s}(\mathbf{q}_{\max.})$ defined by $\omega_0^{c,s}(\mathbf{q}_{\max.}) = \int_0^\infty \omega \mathrm{Im}[\chi^{c,s}(\mathbf{q}_{\max.},\omega)]d\omega / \int_0^\infty \mathrm{Im}[\chi^{c,s}(\mathbf{q}_{\max.},\omega)]d\omega$ in both channels. Inside the superconducting region (indicated by the vertical red dashed lines), the characteristic frequency of the fluctuations are of the order of 100−200 meV. Moreover, $|\omega_0^c$-$\omega_0^s|$ is small and minimal for the region of maximum T_c. In agreement with our discussion above, we see that an increase of V yields even smaller $|\omega_0^c$-$\omega_0^s|$, which suggests that charge and spin contributions to the SC pairing mechanism are cumulative.

Separating spin and charge channels in the pairing mechanism. To disentangle the interplay between charge and spin degrees of freedom in gap Eq. (3), we solve for λ, including contributions from only spin (λ_s) and only charge channel (λ_c), i.e., $V^{\mathrm{eff}}_{\mathbf{q},i\nu_n} = -3W^{\mathrm{s}}_{\mathbf{q},i\nu_n}$ and $V^{\mathrm{eff}}_{\mathbf{q},i\nu_n} = W^{\mathrm{c}}_{\mathbf{q},i\nu_n}$, respectively. First, we follow the phase boundary of the SC phase in the underdoped regime for fixed $V = 0.3$ eV, starting from $(\delta, T) = (0.2, 40\ \mathrm{K})$ up to $(\delta, T) = (0.38, 65\ \mathrm{K})$. In Fig. 4(a) we plot λ, λ_s, and λ_c: Since we are following the phase transition line, $\lambda \approx 1$. λ_c and λ_s are both smaller than λ and $\lambda_c + \lambda_s \approx \lambda$, indicating a *cumulative* charge and spin contribution for the chiral d-wave pairing in the underdoped regime. This observation is surprising and in stark contrast to the expectation that spin and charge fluctuations drive competing instabilities. The same conclusion can be drawn when the λ values are calculated at the critical doping $\delta_c = 0.2$ as a function of the nonlocal interaction V as depicted in Fig. 4(b).

Our data indicates that overall both spin and charge fluctuations are important for the SC phase. As a function of doping, however, we observe that charge fluctuations become increasingly dominant and λ_s becomes negligible. This effect is reflected in the V dependence of the SC dome in Fig. 1, which is stronger at larger dopings. We arrive at the same conclusions

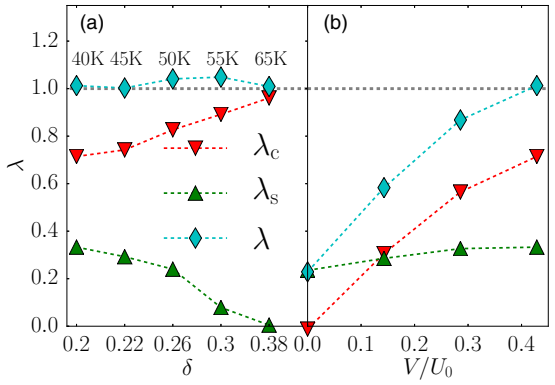

FIG. 4. Eigenvalue λ of the gap equation Eq. (3)(λ = 1 signals SC transition) for full effective singlet pairing interaction $V^{\rm eff}_{\mathbf{q},i\nu_n}$ (cyan) and charge/spin only channels (red/green). (a) Plot for $V = 0.3$ eV along the SC phase boundary up to doping $\delta = 0.38$. (b) Plot as a function of V for fixed doping $\delta = 0.2$ and temperature $T = 40$ K.

when we analyze the dependence of λ on the choice of the Fierz parameter that defines the charge-to-spin fluctuation ratio (Supplemental Material F in Ref. [33]).

Let us stress two important points: (i) The true long-range character is crucial for the predicted SC in silicon adatom materials. If only short-range (i.e., nearest-neighbor) interactions are considered, charge ordering is overestimated and, long before any SC emerges, the system turns into a charge-ordered insulator as proven by calculations shown in the Supplemental Material G in Ref. [33]. (ii) The degeneracy of the $d_{x^2-y^2}$- and d_{xy}-wave-pairing state is important for the cumulative charge and spin interplay. Since the origin of this degeneracy is connected to the lattice symmetry group, a different behavior can be expected for the 2D square lattice (see Supplemental Material H in Ref. [33]): in the square geometry with relatively large V/U_0, the $\mathbf{q}$ dependence of $\chi^{\rm c}(\mathbf{q}, i\nu_n = 0)$ favors $d_{xy}-$pairing symmetry while $\chi^{\rm s}(\mathbf{q}, i\nu_n = 0)$ prefers $d_{x^2-y^2}-$pairing symmetry, and the two channels compete with each other.

IV. CONCLUSION

We predict the existence of a dome-shaped unconventional chiral d-wave superconducting phase for hole-doped triangular lattice systems with $\propto 1/r$ interactions, which could be realized by hole-doping existing α phase Si(111) adatom materials. The analysis of spin and charge correlation functions reveals that lattice geometry as well as the nonlocal interaction are necessary conditions for the emergence of SC. The nature of the pairing undergoes a crossover from an unexpected combined charge/spin mechanism in the underdoped regime toward a charge fluctuation dominated one at higher doping. In future studies, high hole-doping levels will be considered in more detail. Here, triplet $f-$wave pairing symmetry may begin to become important due to the appearance of a disconnected Fermi surface [45].

Note added. During the review process of this paper, we became aware of very recent experimental activities on strongly hole-doped Sn:Si(111). F. Ming. and coworkers [46] were able to reach doping levels up to 10−12% by using boron-doped silicon as a substrate without perturbing the symmetry of the adatom lattice. This first success proves the feasability of synthezising heavily doped adatom systems and motivates further experimental work along the lines of our prediction.

ACKNOWLEDGMENTS

O.P. and T.A. are supported by the FP7/ERC under Grant Agreement No. 278472-MottMetals. We thank Yi Lu, Alessandro Toschi, Ciro Taranto, Thomas Schaefer, and Daniil Mantadakis for helpful discussions.

[1] S. Schuwalow, D. Grieger, and F. Lechermann, Phys. Rev. B **82**, 035116 (2010).
[2] P. Hansmann, L. Vaugier, H. Jiang, and S. Biermann, J. Phys.: Condens. Matter **25**, 094005 (2013).
[3] P. Hansmann, T. Ayral, L. Vaugier, P. Werner, and S. Biermann, Phys. Rev. Lett. **110**, 166401 (2013).
[4] G. Li, P. Höpfner, J. Schäfer, C. Blumenstein, S. Meyer, A. Bostwick, E. Rotenberg, R. Claessen, and W. Hanke, Nat. Commun. **4**, 1620 (2013).
[5] P. Hansmann, T. Ayral, A. Tejeda, and S. Biermann, Sci. Rep. **6**, 19728 (2016).
[6] A. Georges, G. Kotliar, W. Krauth, and M. J. Rozenberg, Rev. Mod. Phys. **68**, 13 (1996).
[7] G. Kotliar, S. Y. Savrasov, K. Haule, V. S. Oudovenko, O. Parcollet, and C. A. Marianetti, Rev. Mod. Phys. **78**, 865 (2006).
[8] Q. Si and J. L. Smith, Phys. Rev. Lett. **77**, 3391 (1996).
[9] G. Rohringer, H. Hafermann, A. Toschi, A. Katanin, A. Antipov, M. Katsnelson, A. Lichtenstein, A. Rubtsov, and K. Held, arXiv:1705.00024 [Rev. Mod. Phys. (to be published)].
[10] T. A. Maier, M. Jarrell, T. Pruschke, and M. H. Hettler, Rev. Mod. Phys. **77**, 1027 (2005).
[11] M. H. Hettler, A. N. Tahvildar-Zadeh, M. Jarrell, T. Pruschke, and H. R. Krishnamurthy, Phys. Rev. B **58**, R7475 (1998).
[12] A. I. Lichtenstein and M. I. Katsnelson, Phys. Rev. B **62**, R9283 (2000).
[13] G. Kotliar, S. Y. Savrasov, G. Pálsson, and G. Biroli, Phys. Rev. Lett. **87**, 186401 (2001).
[14] P. Sun and G. Kotliar, Phys. Rev. B **66**, 085120 (2002).
[15] P. Sun and G. Kotliar, Phys. Rev. Lett. **92**, 196402 (2004).
[16] T. Ayral, S. Biermann, and P. Werner, Phys. Rev. B **87**, 125149 (2013).
[17] A. Rubtsov, M. Katsnelson, and A. Lichtenstein, Ann. Phys. **327**, 1320 (2012).
[18] E. G. C. P. van Loon, H. Hafermann, A. I. Lichtenstein, A. N. Rubtsov, and M. I. Katsnelson, Phys. Rev. Lett. **113**, 246407 (2014).
[19] E. G. C. P. van Loon, M. Schüler, M. I. Katsnelson, and T. O. Wehling, Phys. Rev. B **94**, 165141 (2016).

[20] H. Hafermann, E. G. C. P. van Loon, M. I. Katsnelson, A. I. Lichtenstein, and O. Parcollet, Phys. Rev. B **90**, 235105 (2014).
[21] T. Ayral and O. Parcollet, Phys. Rev. B **92**, 115109 (2015).
[22] T. Ayral and O. Parcollet, Phys. Rev. B **93**, 235124 (2016).
[23] J. Vucicevic, T. Ayral, and O. Parcollet, Phys. Rev. B **96**, 104504 (2017).
[24] T. Ayral, J. Vucicevic, and O. Parcollet, Phys. Rev. Lett. **119**, 166401 (2017).
[25] S. Zhou and Z. Wang, Phys. Rev. Lett. **100**, 217002 (2008).
[26] S.-Q. Su, Z.-B. Huang, R. Fan, and H.-Q. Lin, Phys. Rev. B **77**, 125114 (2008).
[27] K. Kuroki, Phys. Rev. B **81**, 104502 (2010).
[28] R. Nandkishore, L. Levitov, and A. Chubukov, Nat. Phys. **8**, 158 (2012).
[29] K. S. Chen, Z. Y. Meng, U. Yu, S. Yang, M. Jarrell, and J. Moreno, Phys. Rev. B **88**, 041103 (2013).
[30] M. L. Kiesel, C. Platt, W. Hanke, D. A. Abanin, and R. Thomale, Phys. Rev. B **86**, 020507 (2012).
[31] M. L. Kiesel, C. Platt, W. Hanke, and R. Thomale, Phys. Rev. Lett. **111**, 097001 (2013).
[32] A. M. Black-Schaffer, W. Wu, and K. Le Hur, Phys. Rev. B **90**, 054521 (2014).
[33] See Supplemental Material at http://link.aps.org/supplemental/10.1103/PhysRevB.97.155145 for details.
[34] T. Ayral, Ph.D. thesis, Ecole Polytechnique, 2015, https://hal.archives-ouvertes.fr/tel-01247625/.
[35] E. A. Stepanov, A. Huber, E. G. C. P. van Loon, A. I. Lichtenstein, and M. I. Katsnelson, Phys. Rev. B **94**, 205110 (2016).
[36] P. Werner, A. Comanac, L. de' Medici, M. Troyer, and A. J. Millis, Phys. Rev. Lett. **97**, 076405 (2006).
[37] T. Ayral, P. Werner, and S. Biermann, Phys. Rev. Lett. **109**, 226401 (2012).
[38] P. Werner and A. J. Millis, Phys. Rev. Lett. **99**, 146404 (2007).
[39] J. Otsuki, Phys. Rev. B **87**, 125102 (2013).
[40] H. Hafermann, Phys. Rev. B **89**, 235128 (2014).
[41] O. Parcollet, M. Ferrero, T. Ayral, H. Hafermann, I. Krivenko, L. Messio, and P. Seth, Comput. Phys. Commun. **196**, 398 (2015).
[42] A. M. Black-Schaffer, Phys. Rev. Lett. **109**, 197001 (2012).
[43] M. Jarrell and J. Gubernatis, Phys. Rep. **269**, 133 (1996).
[44] P. Werner and M. Casula, J. Phys.: Condens. Matter **28**, 383001 (2016).
[45] K. Kuroki and R. Arita, Phys. Rev. B **63**, 174507 (2001).
[46] F. Ming, T. S. Smith, S. Johnston, P. C. Snijders, and H. H. Weitering, Phys. Rev. B **97**, 075403 (2018).